Progress In Electromagnetics Research B, Vol. 52, 19–36, 2013

PARASITIC CAPACITANCE CANCELLATION OF INTEGRATED CM FILTER USING BI-DIRECTIONAL COUPLING GROUND TECHNIQUE

Hui-Fen Huang and Mao Ye*

School of Electronic and Information Engineering, South China University of Technology, Guangzhou, China

Abstract—This paper introduces a method for canceling the parasitic capacitance of integrated common mode (CM) filter by optimizing the layout of ground winding. Firstly, the CM filter with positive or negative coupling between the ground and inductor winding is researched, respectively. Then, the two coupling polarizes are combined to form the bi-directional coupling, simulation and measured results show bi-directional coupling ground can effectively improve the high frequency (HF) filtering performance. The equivalent circuits are given to demonstrate the cancellation mechanism, and modelling is derived for the design of ground winding. To further validate the application of proposed technique, CM noise and input/output signals for PFC (Power Factor Correction) converter with bi-directional coupling ground CM filter are simulated. The noise spectrums show conductive interference at high frequencies is effectively suppressed and meets the required electromagnetic interference (EMI) standard.

1. INTRODUCTION

Power electronic equipments generate EMI due to high switching dv/dt and di/dt of power switching devices. An EMI filter is widely used to reduce these conducted emissions in practical circuits [1]. As discrete EMI filters have large profiles and poor HF performance, integrated EMI filters have been successfully proposed and implemented to solve these issues [2, 3]. An example structure is illustrated in Figure 1, where parameters L_1, L_2 represent the upper and lower layers of CM inductor windings which are via connected. L_3 represents the ground winding and four terminals A, B, C, D are also marked. Besides, C_p

Received 15 March 2013, Accepted 10 May 2013, Scheduled 21 May 2013

* Corresponding author: Mao Ye (y.mao@mail.scut.edu.cn).

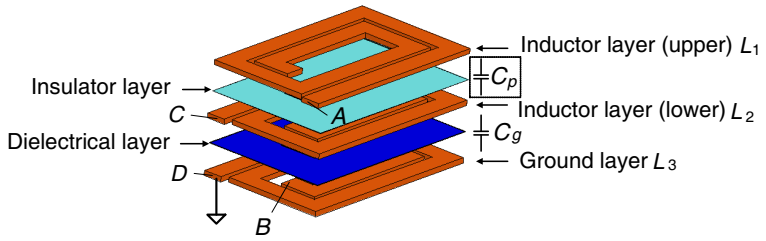

Figure 1. Structure diagram for the CM winding.

is the parasitic capacitance formed by the upper and lower inductor windings. C_g is the CM capacitance formed by the lower inductor winding and the ground winding.

Since the equivalent parallel capacitance (EPC) of the CM inductors C_p leads to self-resonance, attenuation of high frequencies is deteriorated seriously [2]. Many works have been done to reduce the parasitic effect [2–19]. A staggered and interleaving winding structure reduced the parasitic winding capacitance with increased winding complexity and thickness in [3–5]. A grounded conductive layer was embedded between the CM inductor winding coils $L_{(1,2)}$ to achieve EPC cancellation in [6, 7]. Moreover, the techniques realized by extra discrete passive devices are also proposed in [9–17].

As an alternative and convenient solution, the ground winding is newly laid out in this proposed technique, and measured results indicate the resonant frequency brought in by the EPC shifts from kHz to several MHz higher. The effectiveness of the designed CM filter is also validated by simulating the CM noise and input/output signals for PFC converter. Pspice simulation results show that the HF noise suppression is improved and meets the standard. This paper is organized as follows. Section 2 researches the CM filter with uni-directional ground winding which is positively or negatively coupled with the inductor windings. Section 3 researches the CM filter with bi-directional ground winding which both positively and negatively coupled with the CM inductor winding. Finally, Section 4 concludes the paper.

2. RESEARCH FOR CM FILTER WITH UNI-DIRECTIONAL COUPLING GROUND

2.1. Cancellation Mechanism

The equivalent circuit of Figure 1 is shown in Figure 2(a), where the coupling coefficients k_2 and k_3 could be either positive or negative value. By decoupling analysis, the decoupled equivalent circuit of

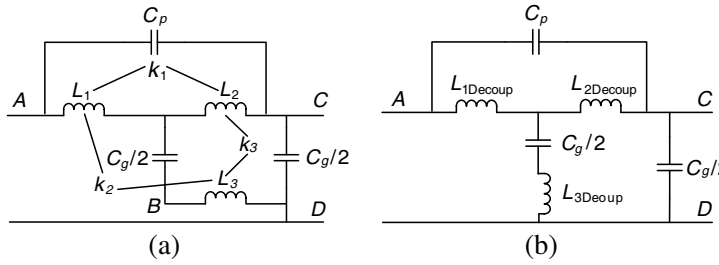

Figure 2. The equivalent circuit for Figure 1: (a) original equivalent circuit, (b) decoupled equivalent circuit.

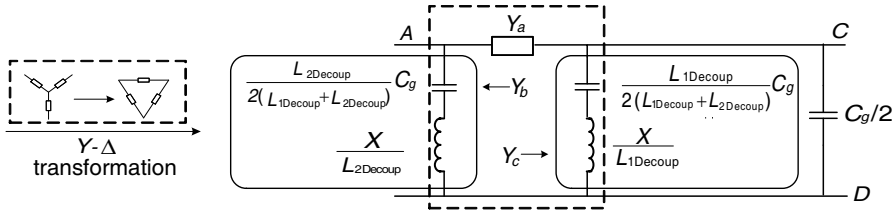

Figure 3. Equivalent π-network.

Figure 2(a) can be seen in Figure 2(b), where the parameters are expressed as follows.

$$L_{1\text{Decoup}} = L_1 + k_1\sqrt{L_1L_2} + k_2\sqrt{L_1L_3} + k_3\sqrt{L_2L_3} \tag{1}$$

$$L_{2\text{Decoup}} = L_2 + k_1\sqrt{L_1L_2} - k_2\sqrt{L_1L_3} - k_3\sqrt{L_2L_3} \tag{2}$$

$$L_{3\text{Decoup}} = L_3 - k_1\sqrt{L_1L_2} + k_2\sqrt{L_1L_3} - k_3\sqrt{L_2L_3} \tag{3}$$

By Y-Δ circuit transformation, the π-equivalent circuit of Figure 2(b) can be referred to Figure 3, where the equivalent admittances are expressed as follows.

$$Y_a = \frac{1 - \omega^2\left[(L_{1\text{Decoup}} + L_{2\text{Decoup}})C_p + L_{3\text{Decoup}}C_g/2\right] + \omega^4 C_p^2 X}{j\omega(L_{1\text{Decoup}} + L_{2\text{Decoup}}) - j\omega^2 C_g X/2} \tag{4}$$

$$Y_b = \frac{j\omega L_{2\text{Decoup}}C_g}{2(L_{1\text{Decoup}} + L_{2\text{Decoup}}) - \omega^2 C_g X} \tag{5}$$

$$Y_c = \frac{j\omega L_{1\text{Decoup}}C_g}{2(L_{1\text{Decoup}} + L_{2\text{Decoup}}) - \omega^2 C_g X} \tag{6}$$

where

$$X = 2L_1\sqrt{L_2L_3}(k_3-k_1k_2)+2L_2\sqrt{L_1L_3}(k_1k_3-k_2)+2L_3\sqrt{L_1L_2} (k_2k_3-k_1)+\left(k_1^2-1\right)L_1L_2+\left(k_2^2-1\right)L_1L_3+\left(k_3^2-1\right)L_2L_3 \quad (7)$$

For the two parallel branches shown in Figure 3, since there exist inductances series connected with the two capacitances, the HF filtering performance could be deteriorated. Taking this into consideration, a small enough value of X is expected in design.

In the integrated structure, since two windings are placed close together on a common axis and high-permeability ferrite core is used, it is easy to get high coupling coefficient. Then $k_{i\,(i=1,2,3)}$ can be assumed ± 1 to simplify the analysis. Then the series admittance of π-equivalent circuit Y_a in (4) can be simplified as:

$$Y_a = \frac{1-\omega^2\left[(L_{1\text{Decoup}}+L_{2\text{Decoup}})C_p+\frac{L_{3\text{Decoup}}C_g}{2}\right]}{j\omega(L_{1\text{Decoup}}+L_{2\text{Decoup}})} \quad (8)$$

In order to make Y_a the admittance of an ideal inductor, it should equal $1/[j\omega(L_{1\text{Decoup}}+L_{2\text{Decoup}})]$, which means that the parasitic capacitance of CM inductor does not exist anymore. According to (8), the ground winding is optimized in order to make C_g satisfy the following condition.

$$C_g = -\frac{2(L_{1\text{Decoup}}+L_{2\text{Decoup}})C_p}{L_{3\text{Decoup}}} = \frac{2(\sqrt{L_1}+\sqrt{L_2})^2C_p}{\sqrt{L_1L_2}\mp\sqrt{L_1L_3}\pm\sqrt{L_2L_3}-L_3} \quad (9)$$

Then Figure 3 can be further specified to an ideal π-shape filter as shown in Figure 4.

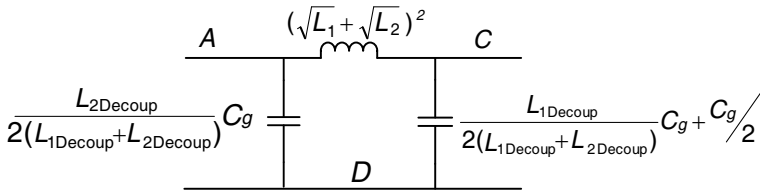

Figure 4. Equivalent circuit with ideal parasitic cancellation.

2.2. Performance Evaluation

The materials used in all researched CM filters are listed in Table 1. The planar E38 + PLT38 cores are made of the material 3E5 with high-permeability. Considering power handle capacity and structural limitation, the width, thickness and distance between adjacent turns

of CM inductor windings are 1.2 mm, 0.3 mm and 0.5 mm, respectively. The thickness of the ground winding is only 0.1 mm.

Table 1. Properties of materials used in HFSS simulation.

Item	Insulation	Dielectric	conductor
Material	Kapton	Ceramic	Copper
Relative Permittivity	3.6	84	1
Thickness (mm)	0.05	0.15	0.3/0.1

For negative coupling ground case, the geometry diagram (top view) of conductor layers in EMI filter with negative coupling ground is shown in Figure 5. The ports are also marked, where L means "line", N "neutral" and G "ground". The current of ground winding is negative couple with current of CM inductor windings. During optimization, the width of ground conductor keeps as 1.2 mm. The parameter L marked in Figure 8 is optimized to satisfy the capacitance value C_g in (9), and the final optimized $L = 37.8$ mm. The designed CM inductance is 4.5 mH, and CM capacitance is 2×1.56 nF in this case.

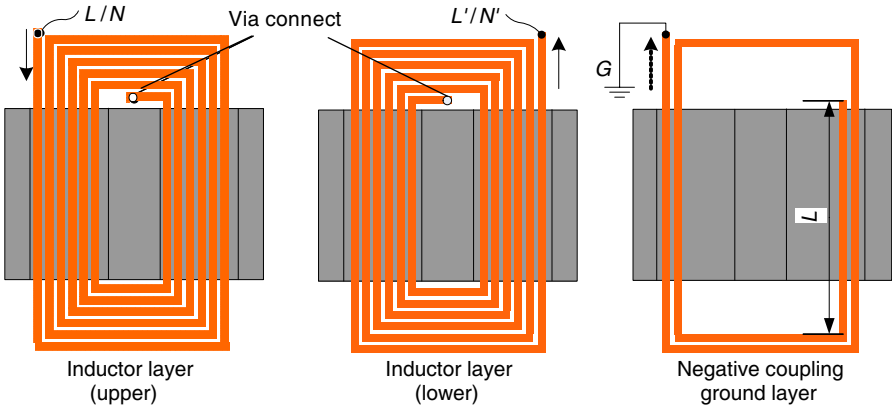

Figure 5. The geometry diagram (top view) of conductor layers in EMI filter with negative coupling ground.

For positive coupling ground case, Table 2 lists the value of C_g corresponding to different number of turns N of ground winding. Finally, $N = 3$ is selected because the corresponding C_g satisfies (9) with the proper size. Figure 6 shows the geometry diagram (top view) of conductor layers in EMI filter with positive coupling ground. The current of ground winding is positively coupled with current of CM

inductor windings. The width parameters of the winding W_1, W_2 and the distance between two adjacent turns Dis are marked in Figure 6, and the optimized $W_1 = 1.65\,\text{mm}$, $W_2 = 4.3\,\text{mm}$, $Dis = 0.5\,\text{mm}$, and $L = 30.05\,\text{mm}$. The designed CM inductance is 4.5 mH, and CM capacitance is $2 \times 3.5\,\text{nF}$.

Simulated insertion losses and phases by Ansoft HFSS simulator are shown in Figure 7. The curves show that the performances of both modified cases are improved compared with the reference curve (with

Table 2. Capacitance C_g corresponding to different N.

N	1	2	3	4	5	6
Capacitance C_g (nF)	2.70	3.06	3.28	3.67	7.46	∞

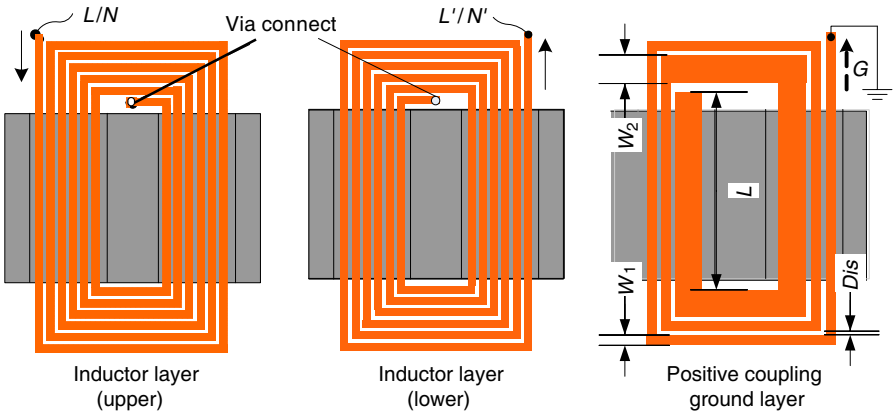

Figure 6. The geometry diagram (top view) of conductor layers in EMI filter with positive coupling ground.

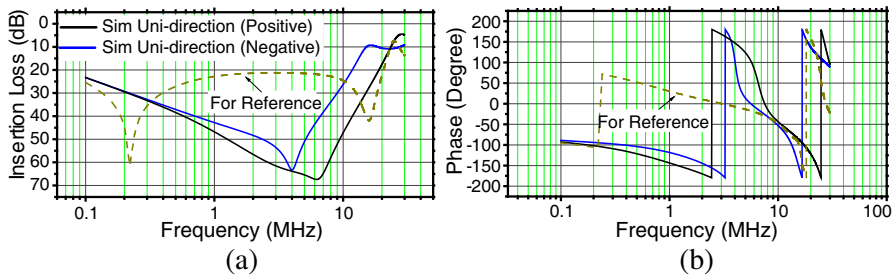

Figure 7. Simulated performance comparisons: (a) insertion losses, (b) phases.

conventional ground). The first-self resonance frequency of CM chokes shifts from 250 kHz to about 5 MHz. Compared with the negative coupling case, the attenuation at several MHz is improved for positive coupling case due to the increased CM capacitance C_g. However, the filtering characteristics are still compromised at higher frequencies.

2.3. Cancellation Effectiveness

In the analysis above, all three couplings are assumed to be ideal. Besides, EPC only represents the first parallel resonance between inductor and the parasitic capacitance. However, these assumptions cannot be satisfied in the real application, especially at high frequencies. Therefore, it is necessary to analyze their influences on cancellation effectiveness.

2.3.1. Non-ideal Couplings

According to (7), the value of X is mainly determined by the three coupling coefficients $k_{i\,(i=1,2,3)}$. To demonstrate this, a Pspice simulatio n is set up as shown in Figure 8. Simulated insertion losses with different coupling coefficients from 0.99 to 1 are depicted in Figures 9(a)–(c). In addition, three special cases are shown in Figure 9(d), where a small enough X is obtained while $k_{i\,(i=1,2,3)}$ not be unity. It can be concluded that coupling coefficients have significant impact on EPC cancellation; the higher value of coupling coefficients, the better HF performance can be achieved.

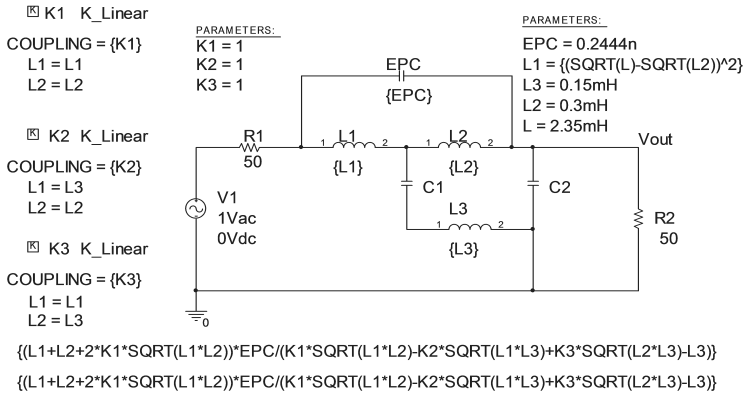

{(L1+L2+2*K1*SQRT(L1*L2))*EPC/(K1*SQRT(L1*L2)-K2*SQRT(L1*L3)+K3*SQRT(L2*L3)-L3)}

Figure 8. Pspice model used for evaluating the influences of coupling coefficients.

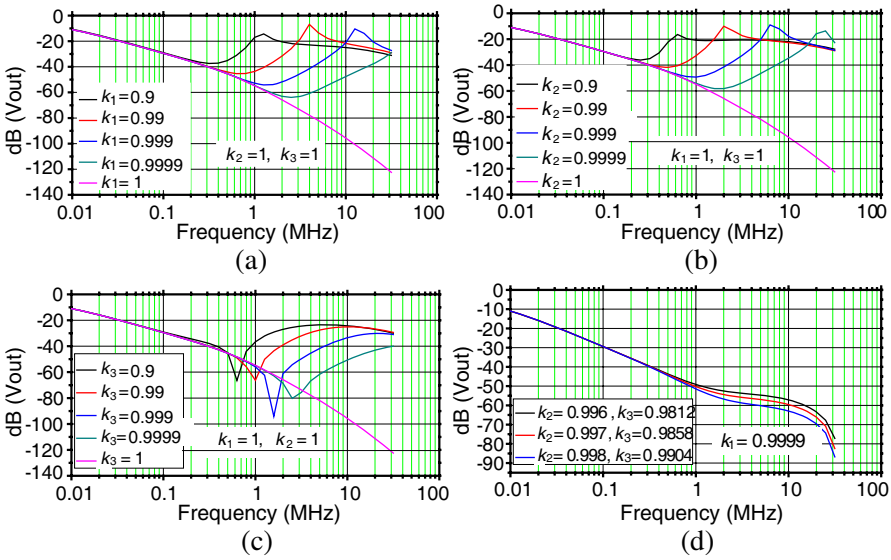

Figure 9. Simulated results which indicated: (a) the influence of k_1, (b) the influence of k_2, (c) the influence of k_3, (d) the special cases of non-ideal couplings ($k_{i\ (i=1,2,3)} \pm 1$).

2.3.2. High-order Resonance

It should be noted that the model given in this paper is only suitable below a certain frequency. As can be seen in Figure 10, divergence appears between the measured and modeled admittance curves of CM inductor prototype at higher frequencies. The higher order resonances arise above 10 MHz and will compromise the cancellation effectiveness.

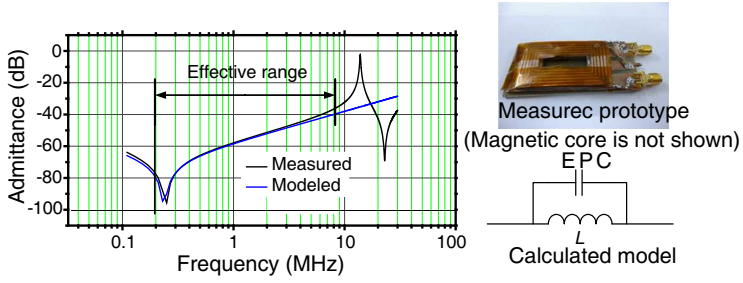

Figure 10. Measured and modeled admittances of CM inductor prototype.

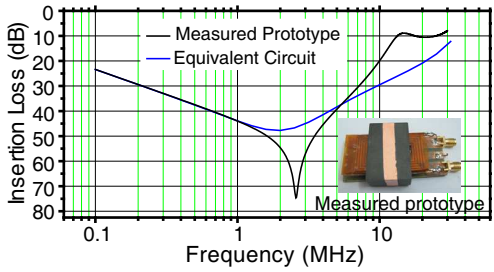

Figure 11. Insertion loss comparison between the equivalent circuit and measured prototype.

To illustrate the validity and limitation of proposed equivalent circuits, Figure 11 shows the insertion loss comparison between the equivalent circuit and measured prototype, and the circuit parameters are listed in Table 3. It can be seen that the two curves will not keep consistent at high frequencies. As discussed, the difference is mainly caused by high-order resonance. Besides, the conductor resistance and parasitic inductance of CM capacitor are also ignored since they have no sufficient influence as EPC. However, the design strategy according to proposed equivalent circuit can still effectively enhance the interference suppression.

Table 3. Circuit parameters.

Parameters	Values
Inductance L_1	0.9707 mH
Inductance L_2	0.3 mH
Inductance L_3	0.15 mH
EPC C_p	244.4 pF
Coefficient k_i	$\pm$0.99991

3. RESEARCH FOR CM FILTER WITH BI-DIRECTIONAL COUPLING GROUND

3.1. Filter Design and Performance Evaluation

The technique in the above section does improve filter performance to a certain degree, but performance at frequencies beyond several MHz is not so good as expected. In this section, the positive and negative

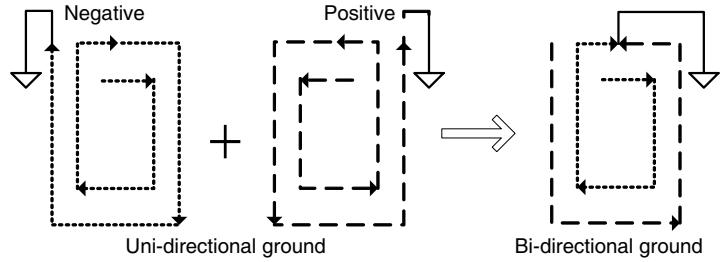

Figure 12. Evolution of bi-directional coupling ground.

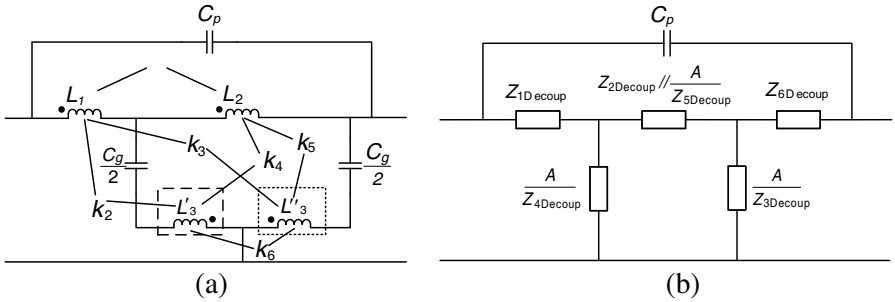

Figure 13. Equivalent circuit: (a) original equivalent circuit, (b) decoupled circuits.

coupling polarizes are combined to form the bi-directional coupling case, as shown in Figure 12. Specifically, the current coupling between one part of ground and CM inductor winding is positive while the other part is negative. Figure 13(a) is the equivalent circuit for the CM filter with bi-directional ground winding. The positive coupling ground coil part L'_3 is marked by long dotted line "- - -", and the negative coupling ground coil part L''_3 is marked by short dotted line "...", $L_3 = L'_3 + L''_3$.

The decoupled circuit of Figure 13(a) can be seen in Figure 13(b). The corresponding parameters are marked in the figures, and

$$Z_{1\text{Decoup}} = j\omega\left(L_1 + \sqrt{L_1L_2} - \sqrt{L_1L_3} - \sqrt{L_2L'_3} + \sqrt{L_1L''_3}\right) \quad (10)$$

$$Z_{2\text{Decoup}} = j\omega\left(L_2 + \sqrt{L_1L_2} + \sqrt{L_1L'_3} - \sqrt{L_2L''_3} + \sqrt{L_2L'_3}\right) \quad (11)$$

$$Z_{3\text{Decoup}} = j\omega\left(L'_3 - \sqrt{L_1L_2} - \sqrt{L_1L'_3} + \sqrt{L_2L'_3} - \sqrt{L'_3L''_3}\right) + \frac{2}{j\omega C_g} \quad (12)$$

$$Z_{4\text{Decoup}} = j\omega\left(L_3'' - \sqrt{L_2 L_3''} - \sqrt{L_3' L_3''} + \sqrt{L_1 L_3''}\right) + \frac{2}{j\omega C_g} \quad (13)$$

$$Z_{5\text{Decoup}} = j\omega\left(\sqrt{L_3' L_3''} - \sqrt{L_1 L_3'}\right), \qquad Z_{6Decoup} = j\omega\sqrt{L_2 L_3''} \quad (14)$$

where

$$A = Z_{3\text{Decoup}} Z_{4\text{Decoup}} + Z_{3\text{Decoup}} Z_{5\text{Decoup}} + Z_{4\text{Decoup}} Z_{5\text{Decoup}} \quad (15)$$

Figure 14 is the geometry diagram (top view) of conductor layers in EMI filter with bi-directional coupling ground. The designed parameters are as follows: $W_1 = 0.8\,\text{mm}$, $W_2 = 1.8\,\text{mm}$, $Dis = 0.5\,\text{mm}$, and $L = 7.5\,\text{mm}$. To clearly demonstrate the integrated structure, Figure 15 shows the half cross-section view of the designed CM filter with bi-directional coupling ground while Figure 16 shows the decomposition diagram.

Figure 17 is the prototype of designed CM filter with bi-directional ground and the measurement setup of CM insertion loss is shown in Figure 18. The measured performance shown in Figure 19 is obtained using Advantest R3770 Network Analyzer. The simulated insertion loss and phase are also displayed. Compared with two uni-directional cases, bi-directional layout further improves the attenuation by 20 dB in the frequency range beyond several MHz. There exists a difference between the simulated and measured curves because the permeability of magnetic core and permittivity of dielectric ceramic may decrease at higher frequencies, while these parameters are assumed to be constant

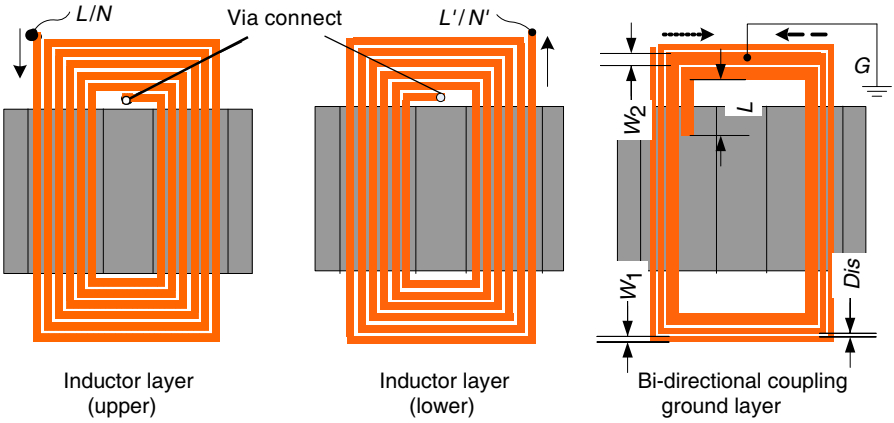

Figure 14. The geometry diagram (top view) of conductor layers in EMI filter with bi-directional coupling ground.

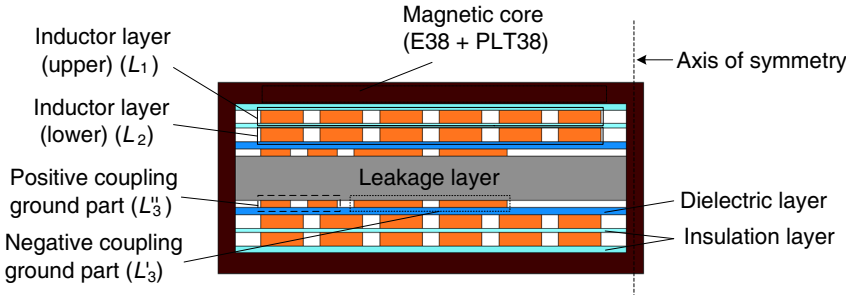

Figure 15. The half cross-section view of designed EMI filter with bi-directional ground.

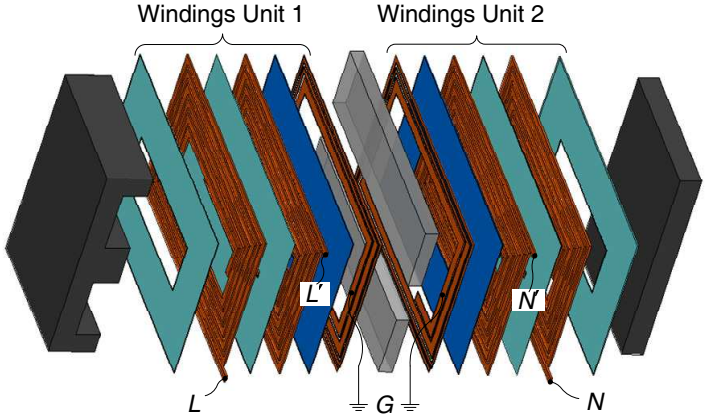

Figure 16. Decomposition diagram of the designed structure.

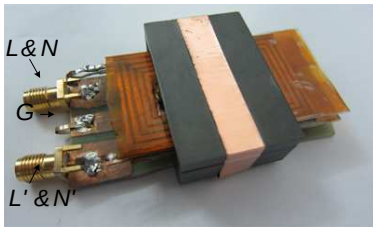

Figure 17. Prototype of the designed CM filter.

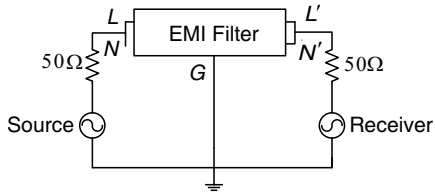

Figure 18. The measurement setup of CM insertion loss.

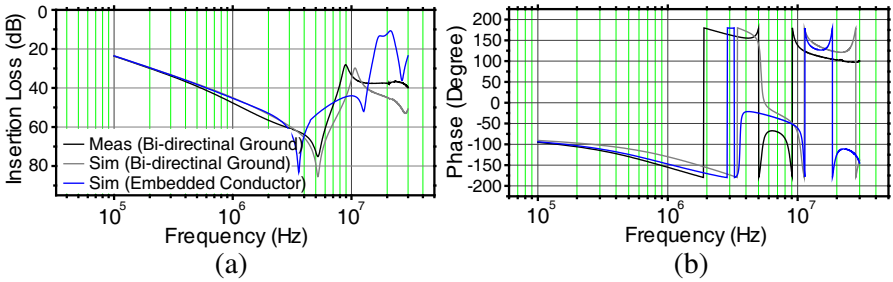

Figure 19. Performance comparisons: (a) insertion loss, (b) phase.

in simulation. Besides, the accuracy of manufacturing process is also an influence factor.

Moreover, the comparison between the proposed method and the "embedded conductor" method can be seen from the insertion loss and the phase comparisons in Figure 19. It is evident that while the proposed integrated CM filter with bi-directional ground did not increase the number of layers, its characteristic is as good as the one with embedded conductor layers over a wider frequency range.

To illustrate the coupling polarity, the current density distributions for the conductor windings are simulated at 1 MHz. Figures 20(a)–(b) show the current distributions for upper and lower inductor windings. Figure 20(c) shows the current distribution of the bi-directional coupling ground winding. It can be seen that there exist reversed direction current distributions in the ground winding, which matches the theoretical analysis. It should be pointed out that the modification of optimizing ground winding does not change different mode (DM) components of the EMI filter; therefore the DM performance will not be affected.

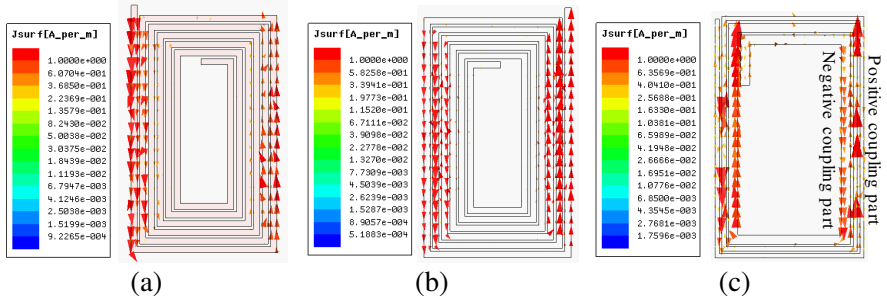

Figure 20. Current density distributions at 1 MHz: (a) upper CM inductor winding, (b) lower CM inductor winding, (c) bi-directional ground winding.

3.2. Application for Power Switching Circuit

To further validate the effectiveness of proposed CM filter, the circuit of PFC converter for a power switching circuit was simulated using the circuit simulator Pspice. The schematic and circuit parameters of the PFC converter for conducted EMI prediction is shown in Figure 21. The MOSFET operating at 200 kHz switching frequency is the main noise sources in switched mode power supplies. As signed, the voltages measured across the two 50 Ω impedances V_L, V_N are defined by the conducted EMI, and the CM noise voltage is expressed as $V_{CM} = (V_L + V_N)/2$.

The noise spectrums from 100 kHz to 30 MHz are derived from time domain simulation followed by FFT analysis, as shown in Figure 22. Comparing the following simulated noise curves: (1) The gray curve shows the noise spectrum when no CM filter is applied; (2) The blue curve shows the noise spectrum when the integrated CM filter with conventional ground is applied; (3) The green curve shows the noise spectrum when the integrated CM filter with proposed

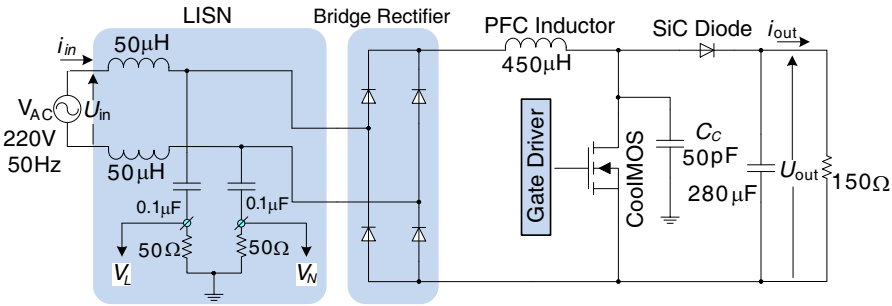

Figure 21. Schematic of FPC converter for conducted EMI prediction.

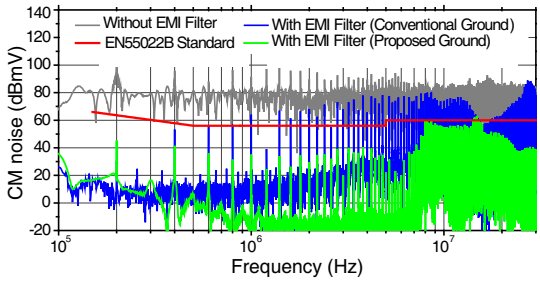

Figure 22. Simulated CM noise spectrums.

ground is applied. Besides, the red curve in this graph indicates the required EN55022 Class B EMI standard. Clearly, the CM conductor noise is above the standard in the entire frequency band for case (1). The CM noise also cannot meet the standard at frequencies beyond several kHz for case (2). Simulation result shows that the noise suppression is greatly improved and meets the standard for case (3), which confirms the effectiveness of the developed parasitic cancellation technique in this paper.

The simulated waveforms of input voltage and input current are shown in Figure 23(a). From this figure, it can be seen that the

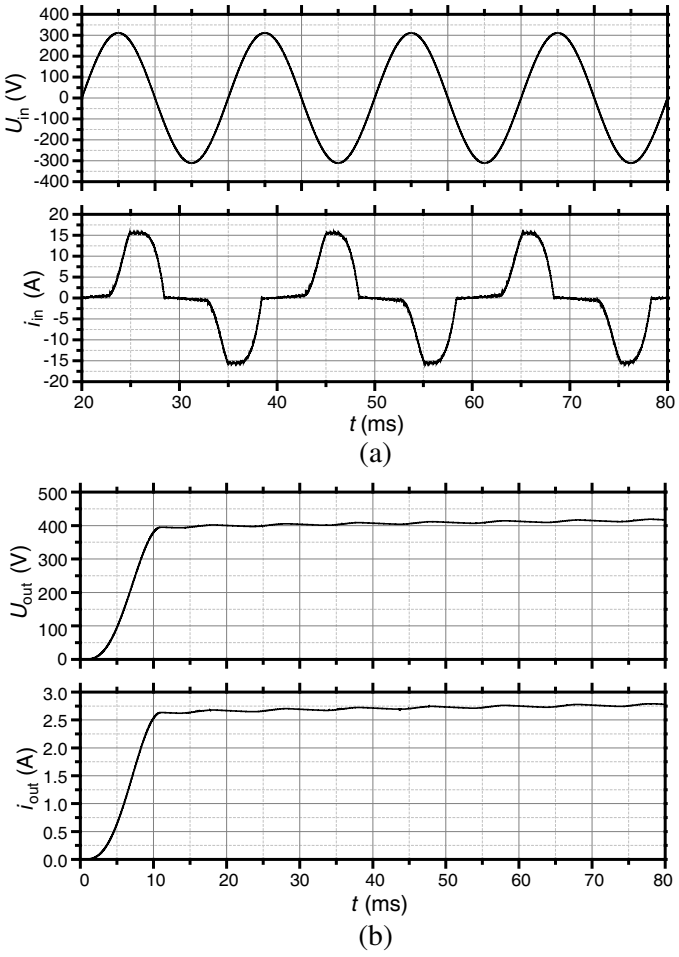

Figure 23. The waveforms of: (a) input voltage and input current, (b) output voltage and output current.

input voltage is standard sine wave and that input current has some harmonics and noise. These harmonics and noise can be effectively reduced by applying an EMI filter connected at the input side of PFC converter. The output voltage and output current of PFC converter with EMI filter are shown in Figure 23(b). As can be seen, the output voltage is almost constant 400 V.

4. CONCLUSION

In this paper, parasitic capacitance of integrated EMI filter is effectively cancelled by using modified ground layer. The simplified equivalent circuits were derived to demonstrate the cancellation mechanism, and main influence factors in implementation were also investigated. Then bi-directional ground winding has been developed and implemented based on the detail analysis of two different uni-directional cases. Simulated and experimental results were presented to confirm the application of proposed technology. In addition, the effectiveness of the CM filter with bi-directional coupling ground is further validated by simulating the CM noise spectrums and input/output signals for PFC converter. Simulation results show that the noise suppression is greatly improved and meets the EMI standard. Since no extra component is required during the design process, the proposed technique is a simple and low-cost way.

ACKNOWLEDGMENT

This project is supported by the National Natural Science Foundation of China (61071056) and Research Fund for the Doctoral Program of Higher Education of China (20090172120009).

REFERENCES

1. Ozenbaugh, R. L., *EMI Filter Design*, 2nd edition, Marcel Dekker, New York, 2001.
2. Lee, F. C., J. D. Van Wyk, Z. X. Liang, R. Chen, S. Wang, and B. Lu, "An integrated power electronics modular approach: Concept and implementation," *Power Electronics and Motion Control Conf.*, 1–13, 2004.
3. Chen, R., "Integrated EMI filters for switch mode power supplies," Ph.D. Dissertation, Virginia Tech, Blackburg, 2004.
4. Chen, R., J. D. Van Wyk, S. Wang, and W. G. Odendaal, "Planar electromagnetic integration technologies for integrated

EMI filters," *Proc. of the IEEE Industry Application Conf.*, 1582–1588, 2003.

5. Chen, R., S. Wang, J. D. Van Wyk, and W. G. Odendaal, "Integration of EMI filter for distributed power system (DPS) front-end converter," *Proc. of the IEEE PESC'03*, 1582–1588, 2003.
6. Chen, R., J. D. Van Wyk, S. Wang, and W. G. Odendaal, "Improving the characteristics of integrated EMI filters by embedded conductive layers," *IEEE Transactions on Power Electronics*, Vol. 20, No. 3, 611–619, May 2005.
7. Jiang, Y., S. Wang, F. C. Lee, and J. D. Van Wyk, "Equivalent parallel capacitance cancellation for noise reduction application," *Applied Power Electronics Conf. and Expo.*, 745–750, 2008.
8. Huang, H.-F. and M. Ye, "Parasitic capacitance cancellation of integrated EMI filter using split ground structure," *Progress In Electromagnetics Research B*, Vol. 43, 91–107, 2012.
9. Wang, S., R. chen, J. D. Van Wyk, F. C. Lee, and W. G. Odendaal, "Developing parasitic cancellation technologies to improve EMI filter performance for switching mode power supplies," *IEEE Transactions on Electromagnetic Compatibility*, Vol. 47, No. 4, 921–929, Nov. 2005.
10. Neugebauer, T. C. and D. J. Perreault, "Parasitic capacitance cancellation in filter inductors," *IEEE Transactions on Power Electronics*, Vol. 21, No. 1, 282–288, Jan. 2006.
11. Wang, S., F. C. Lee, and J. D. Van Wyk, "Design of inductor winding capacitance cancellation for EMI suppression," *IEEE Transactions on Power Electronics*, Vol. 21, No. 6, 1825–1832, Nov. 2006.
12. Wang, S., F. C. Lee, and J. D. Van Wyk, "Inductor winding capacitance cancellation using mutual capacitance concept for noise reduction application," *IEEE Transactions on Electromagnetic Compatibility*, Vol. 48, No. 2, 311–318, May 2006.
13. Wang, S., F. C. Lee, D. Y. Chen, and W. G. Odendaal, "Effects of parasitic parameters on EMI filter performance," *IEEE Transactions on Power Electronics*, Vol. 19, No. 3, 869–877, May 2004.
14. Wang, S. and F. C. Lee, "Common mode noise reduction for power factor correction circuit with parasitic capacitance cancellation," *IEEE Transactions on Electromagnetic Compatibility*, Vol. 49, No. 3, 537–542, Aug. 2007.
15. Wang, S. and F. C. Lee, "Investigating parasitic capacitance

cancellation for EMI suppression," *Vehicle Power and Propulsion Conf.*, 954–961, 2009.

16. Wang, S. and F. C. Lee, "Analysis and applications of parasitic capacitance cancellation techniques for EMI suppression," *IEEE Trans. Industrial Electron.*, Vol. 57, No. 9, 3109–3117, Sep. 2010.
17. Wang, S. and F. C. Lee, "Common mode noise reduction using parasitic capacitance cancellation," U.S. Patent 7602159B2, Oct. 13, 2009.
18. Huang, H.-F., M. Ye, and L.-Y. Deng, "Equivalent parallel capacitance cancellation utilizing coupling between integrated EMI filter components," *PIERS Proceedings*, 1003–1007, Kuala Lumpur, Malaysia, Mar. 27–30, 2012.
19. Huang, H.-F., M. Ye, and S.-Y. Liu, "Equivalent parallel capacitance cancellation of integrated EMI filter using coupled components," *2012 Asia-Pacific Symposium on Electromagnetic Compatibility (APEMC)*, 133–136, 2012.